Adsorption Site Distributions on Cu(111), Cu(221), and Cu(643) as Determined by Xe Adsorption

Layton Baker,[†] Brian Holsclaw,[†] Ashleigh E. Baber,[‡] Heather L. Tierney,[‡] E. Charles H. Sykes,[‡] and Andrew J. Gellman*[,†,§]

Department of Chemical Engineering, Carnegie Mellon University, Pittsburgh, Pennsylvania 15213, United States, Department of Chemistry, Tufts University, Medford, Massachusetts 02155, United States, and National Energy Technology Laboratory, U.S. Department of Energy, P.O. Box 10940, Pittsburgh, Pennsylvania 15236, United States

Received: July 13, 2010; Revised Manuscript Received: September 10, 2010

Xe has been used to probe the distributions of adsorption sites across three different Cu single-crystal surfaces: Cu(111), Cu(221), and Cu(643). These expose terrace, step, and kink sites, respectively. The study couples the use of scanning tunneling microscopy (STM), temperature-programmed desorption (TPD), and photoemission of adsorbed Xe (PAX) to assess their use as methods for determining adsorption site distributions on Cu surfaces. STM shows that the Xe adsorption sites in order of energetic preference are kink, step edge, and terrace, but indicates that the binding energy differences between the three are likely very small. This is borne out by Xe TPD studies that show distinct differences in the desorption kinetics on the three surfaces but unresolvable differences in the desorption temperatures and binding energies at the terrace, step, and kink sites. PAX spectra reveal observable features that can be associated with Xe adsorption at terrace, step, and kink sites. These features can be analyzed semiquantitatively to give insight into the distributions of sites on these surfaces.

1. Introduction

Vicinal single-crystal surfaces are miscut by a small angle relative to a high-symmetry, low-Miller-index crystal plane, and thus, their ideal structures are commonly considered to be composed of low-Miller-index terraces separated by monatomic steps with a specific crystallographic orientation.[1] The steps on many such vicinal surfaces have single-atom displacements in the plane of the terrace to form "kinks". As an example, Figure 1A shows the ideal structure of the Cu(643) surface, a high-Miller-index surface with periodic kinks along the step edges. Terrace, step, and kink sites offer different local geometries for the adsorption of molecules on these surfaces and, therefore, different environments for subsequent surface reactions.

Vicinal surfaces are studied for several reasons. The enhanced catalytic activities of step and kink sites make vicinal surfaces interesting model systems for studies of heterogeneous catalysis. In addition, the presence of steps/kinks can influence how adsorbates behave on the terraces of vicinal surfaces. The atomic structures of vicinal surfaces are investigated to better understand the influence of steps and kinks, as well as their density and orientation, on the morphology and energetics of surface structures. The property of surfaces with kinked step edges that has stimulated the current work is the fact that they are chiral and, hence, can interact enantiospecifically with the two enantiomers of a chiral adsorbate. Kinks on step edges have no mirror plane or rotational symmetry and as a result are "locally" chiral.[2,3] One can think of these kinks as being formed by the intersection of the three low-Miller-index microfacets, and their handedness is dictated by the sense of rotation among these three microfacets as viewed along the surface normal.[3,4] Such naturally chiral metal surfaces exhibit enantioselective interactions with chiral molecules, and thus, chiral metal surfaces can be useful materials for enantioselective catalysis and separations.[3−20] One of the key characteristics of these surfaces that limits understanding of their enantioselective properties is the fact that little is known about their real structures. The ideal structures are those based on the termination of bulk cleavage planes, such as those shown in Figure 1A. Consideration of the ideal structures of chiral surfaces is of limited value because their real structures often differ significantly from the ideal as a result of thermal roughening via atomic diffusion on the surface. Figure 1 shows the ideal structure of an fcc(643)^R surface, the thermally equilibrated structure of a Pt(643)^R surface simulated using kinetic Monte Carlo methods, and a scanning tunneling microscopy (STM) image of the real Cu(643)^R surface.[5,21,22] A cursory glance at Figure 1B,C reveals that the real structure of the surface is markedly different from the ideal structure. As illustrated by the example of the Pt(643)^R surface,[21] to decrease the free energy of the surface, atoms diffuse along the step edges, causing the kinks to coalesce and the straight portions of the step edge to grow in length. This reduces the areal density of kinks. The STM image of the Cu(643)^R surface reveals a real structure that is very similar to that predicted by simulations of thermal roughening on Pt(643)^R. It is important to note that real chiral surfaces maintain the net chirality of their ideal structure despite thermal roughening; that is, the kinks along roughened step edges are formed by the intersection of the three low-Miller-index microfacets with the same sense of rotational orientation as the kinks on the ideal surface structure. One of the consequences of thermal roughening is that the areal densities of different types of adsorption sites on a real surface are different from those on the ideal surface; in general, the density of kinks on the real surface is lower than that on the ideal surface. In addition, the lengths of straight step edges are longer on the roughened surface than on the ideal surface.

* Corresponding author. Phone: 412-268-3848. Fax: 412-268-7139. E-mail: gellman@cmu.edu.
[†] Carnegie Mellon University.
[‡] Tufts University.
[§] U.S. Department of Energy.

10.1021/jp106489f
Published on Web 10/12/2010

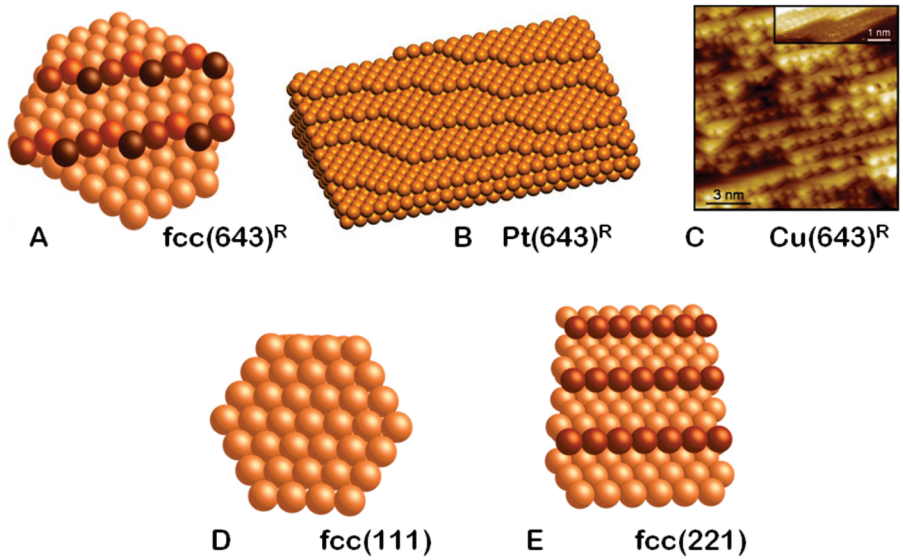

Figure 1. (A) Ideal structure of an fcc(643)^R surface. The (111) terraces are separated by kinked, monatomic steps having 2 × (100) step edges and 1 × (110) kinks. (B) Simulated atomic structure of a Pt(643)^R surface thermally equilibrated at 500 K.[21] Coalescence of the kinks along the step edges reduces the number of kinks and results in the formation of nonideal kinks at the intersections of long step edges; n × (100) and m × (110). The orientation of the microfacets forming the kinks is preserved, and thus, the net chirality of the surface is preserved. (C) STM image of a thermally roughened Cu(643)^R surface at 78 K.[22] The inset shows atomic resolution of one of the nonideal kink sites. Image conditions: $V_{tip} = 0.3$ V, $I = 0.05$ nA. (D,E) Ideal structures of the (D) fcc(111) and (E) fcc(221) surfaces.

Although STM can image these surfaces and provide direct insight into the areal densities of different adsorption sites on the roughened surfaces, a need exists to determine the real atomic structure of vicinal surfaces using spectroscopic tools that sample larger surface areas and are easier to apply than STM.

There are several methods for studying the atomic structure of surfaces. Low-energy electron diffraction (LEED) can be used to study the long-range order of real surfaces over length scales equivalent to the coherence width of the electron beam. LEED experiments can provide information on the average terrace width and step edge orientation. Analysis of I−V curves can be used to determine average step heights, which indicate whether step bunching occurs on a vicinal surface.[23] Recent LEED experiments have also provided some insight into the structures of chiral Pt(531) and Cu(531) surfaces.[24−26] In practice, it is much more difficult to acquire atomically resolved STM images of highly stepped, vicinal surfaces than nominally flat, low-Miller-index surfaces. For this reason, only a few STM studies of highly stepped and kinked (chiral) surfaces have been completed to date.[22,27,28] The work reported in this article explores the use of adsorbed Xe as a probe of local structure on chiral surfaces and the use of temperature-programmed desorption (TPD) and photoemission of adsorbed Xe (PAX) as methods for titrating Xe adsorption sites. Xe is particularly useful as a probe of local surface structure because it is chemically inert and will not induce surface reconstruction.

In PAX, the dependence of Xe 5p photoelectron binding energies on the local work function of the Xe adsorption site can be used to determine the local work function distribution of a heterogeneous surface and, thus, to probe the distribution of different Xe adsorption sites. The PAX method was developed by Wandelt and others, and several reviews of the method are available in the literature.[29−31] The work function of an adsorption site is local in nature and dependent on the local atomic and electronic structure of the surface.[32] The interaction of Xe with substrates is very weak, and thus, initial-state effects on photoelectron binding energies are very small. Furthermore, Xe has a diameter of approximately 4−5 Å and forms a weak bond with substrate atoms and one that is typically 3.5−4.5 Å in length. In this bonding geometry, the center of an adsorbed Xe atom is outside the electrostatic surface potential, and thus, the Xe electron binding energies are pinned to the vacuum level; E_B^{vac} is independent of adsorption site. When electron potentials are pinned to the vacuum level, the observed binding energies relative to the energy of the Fermi level, E_B^F, as measured in a photoemission experiment, will be influenced by the local work function, ϕ_{loc}

$$E_B^F + \phi_{loc} = E_B^{vac} \quad (1)$$

If two adsorption sites (i and j) have different local work functions, then there will be an equal, but opposite, difference in the observed binding energies of Xe $5p_{1/2}$ photoelectrons originating from these two sites.

$$E_B^F(i) - E_B^F(j) = \phi_{loc}(j) - \phi_{loc}(i) \quad (2)$$

Numerous experimental and theoretical studies of Xe on Cu surfaces and many other surfaces have been reported in the literature.[33] Most studies of Xe adsorption and dynamics on Cu have been performed on the nominally flat (111), (100), and (110) surfaces.[34−40] Building on this work, we report herein studies of Xe adsorption on the flat Cu(111), stepped Cu(221), and chiral Cu(643) surfaces using STM, TPD, and PAX to attempt to titrate the density of terrace, step, and kink adsorption sites on these three surfaces. The ideal structures of these surfaces are shown in Figure 1A,D,E. The Cu(221) surface has terraces formed by (111) microfacets and straight, monatomic step edges formed by (110) microfacets. The Cu(643) surface has terraces formed by (111) microfacets and kinked step edges formed by (100) steps and (110) kinks. The work reported in this article uses Xe adsorption to probe the real, thermally roughened surface structures and the differences in densities of terrace, step, and kink adsorption sites on the Cu(111), Cu(221), and Cu(643) surfaces.

2. Experimental Section

2.1. STM. All STM experiments were performed in a low-temperature, ultra-high-vacuum (LT-UHV) STM instrument (Omicron). The Cu(643) crystal was sputtered with Ar^+ ions (1.5 keV at 13 μA) for 30 min and then annealed for 2 min to 1000 K.[22] After the final anneal, the crystal was transferred in less than 4 min and in vacuum ($<5 \times 10^{-10}$ Torr) to the precooled STM sample chamber. Within 30 min, the sample was cooled to 78 K (or 7 K). The Cu(111) single crystal used for the STM experiments was purchased from MaTecK and cleaned by cycles of Ar^+ ion sputtering (1 keV at 13 μA) and annealing at 760 K. The STM scanner was equipped with a sample heater capable of heating both the tip and sample to 50 K above the base temperatures of either 7.7 K (using liquid He) or 78 K (liquid N_2). This feature allowed the study of adsorbate diffusion in a particular area of the surface over a fairly wide temperature range. Xe gas (99.995% purity) was purchased from Airgas and adsorbed directly onto the sample at 7.7 K using a collimated molecular doser connected to a leak valve. The Xe coverage was calculated from the STM images, and a coverage of 1 ML of Xe formed the $(\sqrt{3} \times \sqrt{3})R30°$ Xe overlayer structure.

2.2. Xe TPD and PAX. The Cu(643) crystal used in the STM experiments was prepared in a similar fashion and then studied using PAX and TPD in a different UHV apparatus. The TPD and PAX experiments were performed in an ultra-high-vacuum (UHV) system pumped by means of stacked turbopumps to a base pressure of $<10^{-10}$ Torr. A typical background pressure during experiments was 5×10^{-11} Torr. Xe TPD and PAX were also performed on Cu(111) and Cu(221) surfaces prepared in the same manner as the Cu(643) surface. The crystals were mounted on a vacuum sample manipulator by means of 1 mm Ta wires spot-welded to opposite edges of the sample disks. The Ta wires were attached to copper blocks mounted onto the cold-head of a closed-cycle Gifford−McMahon cyro-refrigerator (Cryomech AL10). The sample temperature was monitored by means of a type-K thermocouple spot-welded directly to the top edge of the crystal. The design of the sample holder/manipulator was such that Cu samples could be cooled to 50 K and resistively heated to over 1100 K.

The Cu crystal surfaces were cleaned by cycles of sputtering (Ar^+, 2.5 keV) and annealing to 1000 K prior to experiments. Clean sample surfaces were characterized by sharp LEED patterns with low inelastic background and the absence of detectable contaminants.

TPD of Xe was performed using an Extrel quadrupole mass spectrometer. The crystal surfaces were exposed to Xe gas (99.995% UHP from Spectra Gases) by positioning the crystal surface in front of a leak valve fitted with a stainless steel dosing tube. The samples were then positioned in front of the aperture to the mass spectrometer for TPD measurements. A constant heating rate of 0.5 K/s was used in all Xe TPD experiments, and the sample temperature was maintained within ±0.3 K of the set point during sample heating.

PAX was performed using a Specs 10/35 He(I) photon source and a Specs Phoibos 150 MCD hemispherical electron energy analyzer. The analyzer was operated with an acceptance angle of ±3° and an energy resolution $\Delta E < 80$ meV. Further reduction of the nominal energy resolution did not improve the resolution of the PAX spectra as determined from the full width at half-maximum (fwhm) of the Xe $5p_{1/2}$ and Cu d-band states. To obtain PAX spectra at increasing coverages of Xe, the spectra were obtained during adsorption of Xe onto the surface. In other words, the spectra were obtained with a background pressure of Xe ($\sim 10^{-9}$ Torr) while the sample temperature was held at ~55 K.

3. Results

3.1. Scanning Tunneling Microscopy. Figure 1C shows an STM image of the $Cu(643)^R$ surface recorded at 78 K.[22] Because of the very high step density on the Cu(643) surface, imaging of the surface by STM was very difficult and required a tip with a high aspect ratio. Good-quality images were obtained by applying 10 V pulses to the tip while scanning different parts of the crystal until a sharp, stable tip was achieved. When compared to the structure of the ideal Cu(643) surface (Figure 1A), it is evident that the real surface has undergone significant roughening via thermal diffusion to lower the surface free energy, as predicted by simulations. In fact, the image is qualitatively similar to that predicted by molecular simulations of roughening of the Pt(643) surface (Figure 1B).[21] The terraces are inhomogeneous in size, and the kinks are spaced unequally along the step edge. Furthermore, as indicated in the inset to Figure 1C, the kinks can occur at the intersections of long, nonideal step edges. Although thermal roughening reduces the areal density of kinks on the real surface relative to that on the ideal structure, it is important to note that the kinks all have the same orientation and, thus, the net chirality of the surface is maintained. Atomic-resolution imaging, as shown in the inset in Figure 1C, reveals that all of the kinks are of the same chirality.[22] This observation is consistent with both theoretical predictions noted above and STM studies of other chiral surfaces.[21,27,28]

Although the Cu(111) surface was nominally flat, all such surfaces contain some residual steps as a result of slight, local misorientation of the crystal surface. Although Cu(111) has no net chirality, locally its step edges contain both R and S kinks. Therefore, with its wide terraces separating monatomic step edges that contain equal numbers of R and S kinks, Cu(111) is an ideal surface on which to study the temperature dependence of Xe adsorption at step edges. Figure 2 shows STM images obtained at 7.7 K of atomically resolved and isolated Xe atoms adsorbed at the bottom of the step edges of Cu(111). Figure 2A shows images obtained at very low Xe coverage at which the Xe atoms adsorb preferentially at the kink sites. The inset of Figure 2A shows an isolated Xe atom adsorbed at a kink site. The topographic height of the Xe atoms measured 0.22 nm, consistent with that expected for Xe atoms adsorbed at sites below the step edge.[39] As the coverage was increased, the Xe began to populate the straight parts of the step edge (Figure 2B). The features observed running parallel to the step edges in the STM images are electron standing waves originating from scattering of the surface-state electrons from the step edges. It is evident from Figure 2 that the kink sites on step edges are the preferred Xe adsorption sites at 7.7 K. Figure 2A also reveals that, once kinks sites are filled, the Xe appears to adsorb at the step edges by binding at sites adjacent to other Xe atoms, thus forming rows at the bottom of the step edge. Higher-coverage data (not shown) reveal that, once all of the sites below the step edges are filled, two-dimensional (2D) island growth begins both around the step edges and on the terraces. These data show that the binding site preference of Xe on Cu(111) surfaces is kinks > straight step edges > terraces, consistent with the observations of Park et al.[39] These results also reveal that, when adsorbed on the surface at 7.7 K, Xe is sufficiently mobile to diffuse across the terraces and along the step edges to find its preferred adsorption sites.

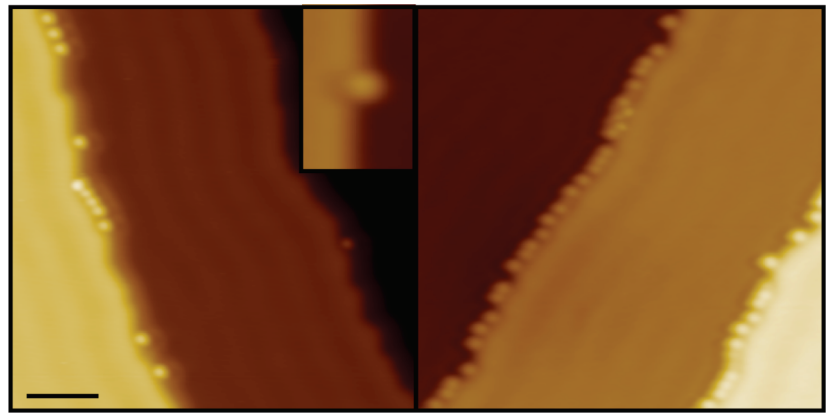

Figure 2. STM images of Xe adsorption at step edges on a Cu(111) surface. (Left) Obtained at low Xe coverage ($\theta_{Xe} = 1 \times 10^5$ ML); Xe adsorbs preferentially at the kink sites on the lower side of the step edges. The inset on the left shows a single Xe atom adsorbed at a kink site. Scale bar = 3 nm. (Right) Image revealing that, at higher Xe coverage ($\theta_{Xe} = 4 \times 10^{-4}$ ML), all of the sites below the step edges become occupied by Xe. Image conditions: (left) $V_{tip} = 0.01$ V, $I = 0.05$ nA, $T = 7.7$ K; (inset) $V_{tip} = 0.001$ V, $I = 0.01$ nA, $T = 7.7$ K; (right) $V_{tip} = 0.001$ V, $I = 0.01$ nA, $T = 7.7$ K.

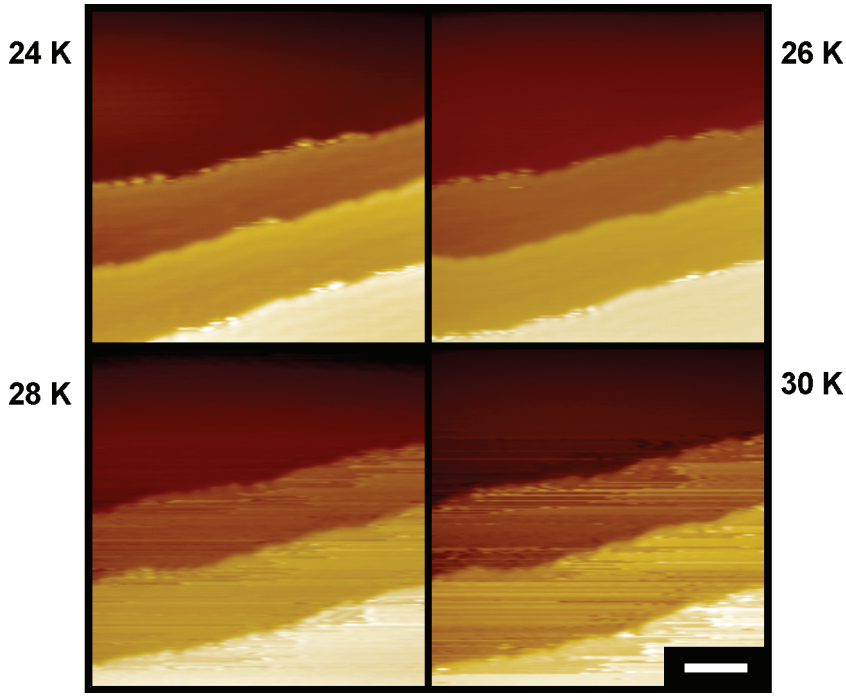

Figure 3. STM images of the temperature-dependent mobility of Xe atoms adsorbed at step edges on a Cu(111) surface. At $T \leq 26$ K, Xe atoms are adsorbed preferentially at step edges. As the temperature increases, the Xe atoms acquire enough thermal energy to populate the Cu(111) terraces. Image conditions: $V_{tip} = 0.01$ V, $I = 0.01$ nA, Xe coverage $= 3 \times 10^{-4}$ ML. Scale bar is 4 nm.

To determine the temperature dependence of the distribution of Xe atoms among adsorption sites, STM images were obtained of Xe at low coverages on Cu(111) over a wide temperature range. As a result of Xe's unique electronic structure, it is only possible to image Xe atoms at very low biases and high currents.[39,41,42] This is problematic because Xe is weakly bound to metal surfaces and can be easily moved by the STM tip.[43,44] Therefore, before each experiment, the scanning conditions were chosen to maximize the image quality, and care was taken to check that the STM tip did not perturb the Xe atoms over many scans so that thermally induced diffusion could be differentiated from tip-induced motion. To investigate the effect of temperature on the distribution of Xe atoms on the surface, a step edge populated by Xe was found and imaged repeatedly as the sample warmed. Corrections for thermal drift allowed continuous monitoring of the same area of the surface over a temperature range of ~30 K. Figure 3 shows Xe atoms adsorbed at three step edges as a function of temperature. A dramatic change in the images was observed at temperatures between 26 and 28 K. The terraces that were imaged clearly at ≤26 K became streaky, and line scans revealed that the topographic height of the noise was equal to the topographic height of Xe atoms (~0.22 nm). This phenomenon indicates the detachment of Xe from the step edges and the formation of a 2D gas in which atoms or molecules adsorbed on terraces are mobile and STM images appear streaky as the adsorbates are diffusing on a time scale faster than that of imaging.[45] In the present case, Xe atoms that are adsorbed preferentially at the step edges at $T < 26$ K occupy a distribution of terrace and step edge sites at $T > 28$ K. At low temperatures, enthalpy favors adsorption at the step edges; however, at higher temperatures, the significant width of the terraces entropically favors adsorption on the terraces.

As the Xe coverage was increased, hexagonal islands of Xe atoms began to form on the Cu(111) terraces, as seen in Figure

4. The sides of the islands were rotated by 30° relative to the atomic lattice of the Cu(111) substrate, consistent with previous work showing that Xe packs in a $(\sqrt{3} \times \sqrt{3})R30°$ structure on Cu(111).[46] The thermal stability of these islands was investigated by imaging the same area of the surface as the substrate temperature was slowly increased. The size of the Xe islands appeared static on time scales of 1 h at $T \leq 20$ K. At higher temperatures, they began to fluctuate. Figure 4 shows an example of this behavior in which three islands coalesce into one large island. This is an example of Ostwald ripening in which atomic mobility on the surface leads to shrinking of small 2D solid islands and growth of the large islands. The mechanism for such rearrangement begins with detachment of atoms having the fewest nearest neighbors from the edges of the small islands; these have the lowest energetic barrier to leaving the island and joining the 2D gas on the terrace. These mobile atoms then diffuse around the terraces until they coalesce with another island. Through this process, the large islands grow, and the smaller ones shrink.

3.2. Temperature-Programmed Desorption of Xe. TPD experiments were performed on Cu(111), Cu(221), and Cu(643) for initial coverages of Xe ranging from a few percent of a monolayer to multiple adsorbed layers. The TPD spectra are shown in Figure 5 for initial Xe coverages up to 1 ML.

On Cu(111), Xe exhibits zeroth-order desorption kinetics except at very low coverage. Over most of the coverage range, the desorption peak temperature increases with increasing coverage, and the leading edges of the desorption features overlap one another. At coverages greater than a few percent of a monolayer, Xe forms 2D solid islands (as shown in Figure 4) that exist in a thermodynamic equilibrium with a 2D gas phase of individual Xe atoms. A simple model for Xe desorption from nominally flat surfaces is that Xe desorbs from the 2D gas phase and not the 2D solid phase, so that the rate of desorption, r_{des}, is first-order with respect to the concentration of Xe in the 2D gas phase, θ_{Xe}^{gas}.

$$r_{des} = k\theta_{Xe}^{gas} \tag{3}$$

The equilibrium between Xe in the 2D solid islands and Xe in the 2D gas effectively keeps the value of θ_{Xe}^{gas} constant during the desorption process until, at low total Xe coverages, no 2D solid islands remain. Then, Xe desorption exhibits first-order behavior with respect to the total Xe coverage. Using zeroth-order desorption kinetics, the Arrhenius desorption energy from Cu(111) was estimated to be approximately $\Delta E_{des} = 0.23$ eV/atom or 22 kJ/mol, based on a monolayer desorption peak temperature of 81 K and a using pre-exponential factor of $\nu \approx 10^{15}$ s^{-1} determined previously for Xe desorption from Ag(111).[47]

TPD of Xe from the Cu(221) surface immediately reveals the impact of steps on the Xe desorption kinetics (Figure 5). The Cu(221) surface has terraces formed by the (111) facet and step edges formed by the (110) facet (Figure 1E). Xe desorption kinetics on Cu(221) are clearly not zeroth-order with respect to Xe coverage. Xe desorption is roughly first-order at low coverage and then tends toward zeroth-order behavior at high coverage. At the lowest coverages, the desorption peak temperature on Cu(221) was approximately 80 K, which is slightly higher than on Cu(111) (approximately 77 K). As shown by STM in this study, at temperatures above 28 K, sufficient thermal energy is available for Xe to detach from step edges and diffuse onto the terrace, and equilibrium exists between Xe adsorbed at step edge sites and Xe adsorbed on the terrace. At 28 K, $k_B T = 0.23$ kJ/mol, which is roughly 1% of the ΔE_{des} value determined for Xe on Cu(111). These factors indicate that the energy difference between step and terrace adsorption sites

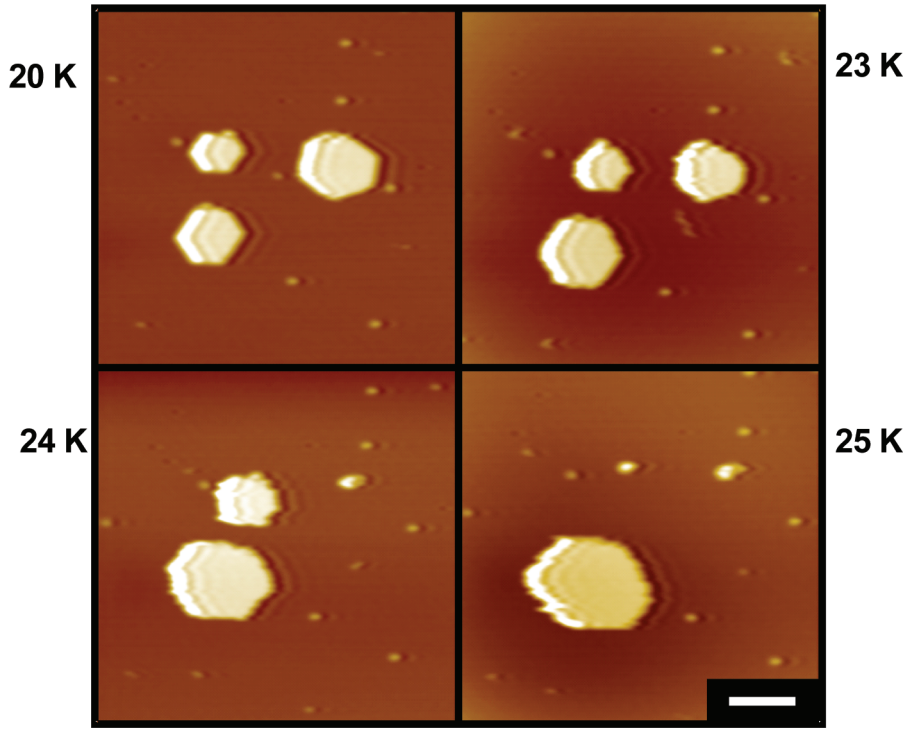

Figure 4. STM images of the temperature-dependent mobility of Xe islands on the Cu(111) surface. At $T < 20$ K, Xe forms stable $(\sqrt{3} \times \sqrt{3})R30°$ islands on the (111) terraces. As the temperature is increased, Xe atoms at the edges of the islands become mobile, and Ostwald ripening leads to the annihilation of small islands and growth of larger ones. Image conditions: $V_{tip} = 0.3$ V, $I = 0.1$ nA, Xe coverage = 0.04 ML. Scale bar is 8 nm.

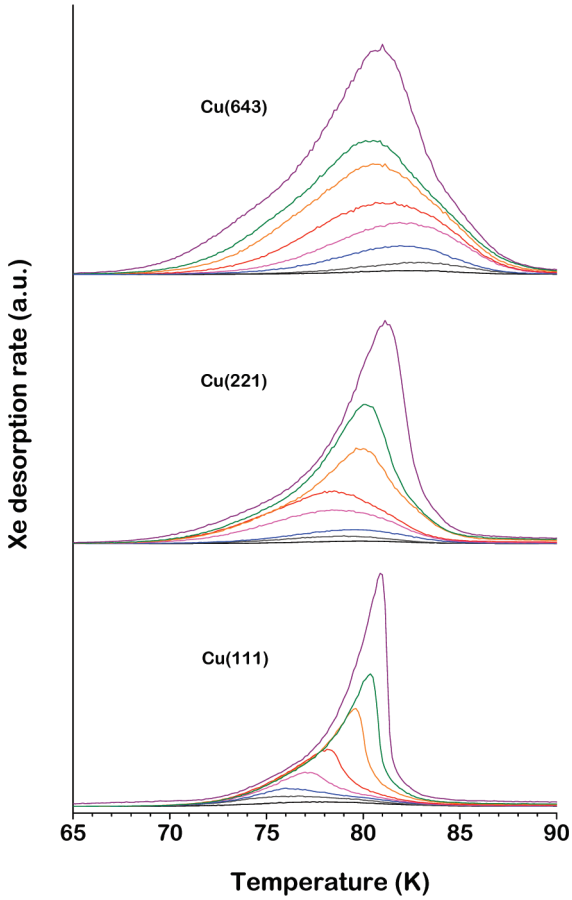

Figure 5. TPD spectra of Xe on Cu(111), Cu(221), and Cu(643) for initial Xe coverages from 0.01 to 1 ML. Xe adsorption was performed at $T < 60$ K. The temperature range over which Xe desorbs was found to be very similar on all three surfaces. Desorption kinetics shift from zeroth-order on Cu(111) to roughly first-order on Cu(643). Spectra for the three surfaces are offset for clarity. The heating rate was 0.5 K/s.

is very small relative to ΔE_{des} for Xe. During TPD experiments, it is likely that Xe detaches from step and kink adsorption sites prior to desorption. As such, the steps have little influence on the desorption energetics, but have a significant impact on the apparent order of desorption.

Desorption of Xe from the Cu(643) surface is clearly not zeroth-order. It appears that the smaller terraces enhance the first-order behavior of Xe desorption. The Xe desorption spectra are indicative of a distribution of heterogeneous adsorption sites that exhibit first-order desorption kinetics with respect to Xe coverage. Although there are kink adsorption sites on the Cu(643) surface, as shown in the STM image (Figure 1C), there is no clear feature in the desorption spectra that would indicate Xe desorbing from kink adsorption sites.

Examination of the TPD spectra for very low coverages of Xe can be used to estimate the desorption energetics under conditions of first-order desorption at which 2D island formation and Xe−Xe interactions are absent. The desorption spectra for 0.02−0.03 ML coverages of Xe on the three surfaces are shown in Figure 6. At these low coverages, Xe desorption kinetics are first-order, as expected, because solid 2D islands of Xe do not form on the surfaces. There are small differences in the low-coverage desorption peak temperatures: 78 K on Cu(111), 80 K on Cu(221), and 82.5 K on Cu(643). These small shifts in peak temperature at low coverage indicate, once again, that the adsorption energies of Xe at kink, step, and terraces sites differ by ~1 kJ/mol.

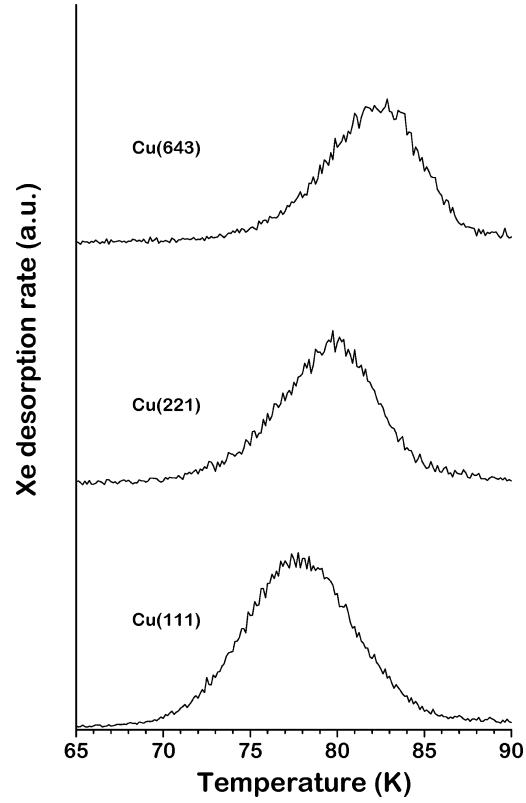

Figure 6. TPD spectra of Xe on Cu(111), Cu(221), and Cu(643) for initial Xe coverages of 0.02−0.03 ML. Xe was adsorbed at $T < 60$ K. At low coverage, Xe desorption kinetics are first-order on all three surfaces. The desorption peak temperatures of 78 K on Cu(111), 80 K on Cu(221), and 82.5 K on Cu(643) indicate that there are small differences in adsorption energies on terrace, step, and kink adsorption sites. The heating rate was 0.5 K/s.

3.3. Photoemission of Adsorbed Xe. PAX was used to gain insight into the adsorption site distribution of Xe on the Cu(111), Cu(221), and Cu(643) surfaces. PAX was performed for Xe adsorbed at coverages ranging from 0 to 1 ML and at temperatures in the range of ~55 K. PAX spectra focusing on the Xe $5p_{1/2}$ and $5p_{3/2}$ emission features for all three surfaces and over the full range of coverages are shown in Figure 7. Spectra were obtained with the photon incident at an angle of ~45° from the surface normal and emission angles of 10−15° from normal. The sample manipulator has a limited range of motion and angular orientation. As such, the spectra for each surface were acquired at different emission angles with respect to the crystallographic axes of the substrate. This limits the direct comparisons that can be made between the spectra for the three surfaces because electron binding energies of valence states in substrates and adsorbates can be emission-angle-dependent due to dispersion of the valence states within the Brillouin zone. Thus, caution is required when comparing the absolute values of the electron binding energies of Xe, E_B^F, between surfaces. However, spectral components within the three sets of spectra and the relative intensities of components are valuable.

On Cu(111), one dominant Xe $5p_{1/2}$ component is observed at $E_B^F(5p_{1/2}) = 7.28$ eV. This peak is attributed to photoemission from solid 2D islands of Xe adsorbed on (111) terraces. In addition, a small shoulder is observed at $E_B^F(5p_{1/2}) = 7.53$ eV. The shoulder is attributed to Xe adsorbed at defect sites, such as step edges on the surface. From analysis of the PAX spectra, the ratio of the terrace to step Xe peak areas shifts from approximately 0.5 at a coverage of $\theta_{Xe} = 0.04$ ML to 6 at $\theta_{Xe} = 1$ ML. This is consistent with STM observations indicating

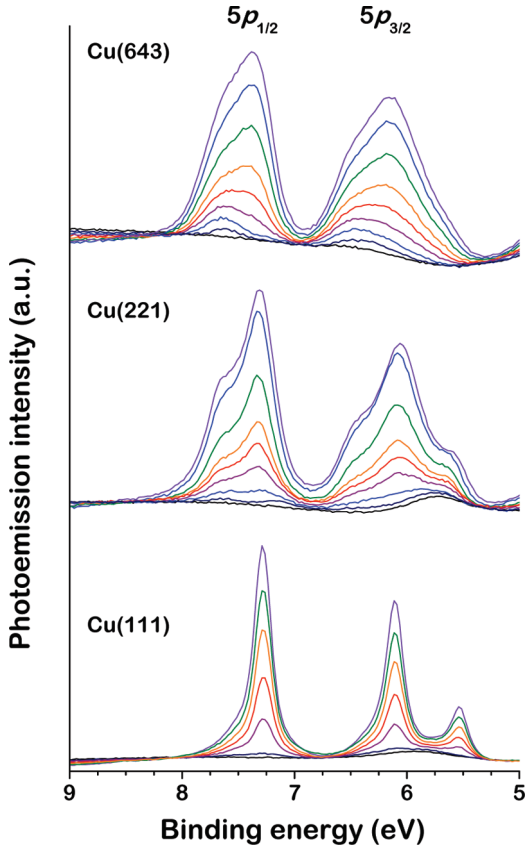

Figure 7. PAX spectra of Cu(111), Cu(221), and Cu(643) surfaces with Xe coverages in the range from <0.1 to 1 ML. Xe adsorbed at the step and kinks sites on Cu(221) and Cu(643) yields the high-binding-energy features on the $5p_{1/2}$ and $5p_{3/2}$ peaks that do not appear in the PAX spectra from the Cu(111) surface. PAX spectra were obtained at $T = \sim 55$ K.

that Xe preferentially adsorbs at step edge sites, even when sufficient thermal energy is available for Xe detachment from the step. It is important to note that neither the step nor terrace peaks saturate in intensity until $\theta_{Xe} \approx 1$ ML, indicating that there is a rapid equilibrium between Xe atoms adsorbed at step edges and on terrace sites at 50 K.

On Cu(221), two distinct Xe $5p_{1/2}$ states are observed. The dominant component at $E_B^F(5p_{1/2}) = 7.28$ eV is due to photoemission from Xe adsorbed on (111) terrace sites. The broad feature at $E_B^F(5p_{1/2}) = 7.60$ eV arises from Xe adsorbed at the step edges and kinks. In contrast with the Cu(111) surface, analysis of the PAX spectra from Cu(221) shows that the ratio of terrace to step peak area is roughly 0.5 and does not change significantly with increasing θ_{Xe}.

In the PAX spectra obtained from the Cu(643) surfaces, it is difficult to clearly distinguish Xe $5p_{1/2}$ states that arise from terrace, step, and kink adsorption sites. With a high density of kinks on the surface, it is likely that there is a distribution of kink and step adsorption site types, with slightly varying local work functions. For instance, thermal roughening leads to the formation of kinks at the intersections of long (100) and (110) step edges. This being the case, analysis of the spectra and decomposition into component peaks is, perhaps, somewhat more arbitrary for Cu(643) than for Cu(111) and Cu(221). Nonetheless, visual inspection of the PAX spectra from Cu(643) suggests that, at low values of θ_{Xe}, there is a preference for Xe binding at the kinked step edges, with subsequent population of the terrace sites. As observed for Cu(111) and Cu(221), the different component peaks on Cu(643) do not saturate until $\theta_{Xe} = 1$ ML. In other words, population of the kinked step edges and the terraces sites is not purely sequential; they are populated concurrently as θ_{Xe} is increased but with a coverage-dependent probability.

4. Discussion

One of the primary goals of the work presented here, and of similar work using Xe adsorption, has been to titrate the distribution of adsorption sites on surfaces with poorly defined or undetermined structures. Even single-crystalline metal surfaces have imperfectly defined structures, in the sense that thermal roughening and other imperfections lead to nonideal structures (Figure 1B,C). This work has used STM, Xe TPD and PAX as probes of surface structure on three Cu surfaces of increasingly complex surface structure: Cu(111), Cu(221), and Cu(643). Although the data clearly reveal sensitivity to surface structure, the question is: What level of quantification is possible, and which of these methods are most informative? In principle, STM provides real-space images that can be analyzed to determine terrace, step, and kink site densities; however, obtaining such images and subsequently analyzing them is nontrivial. Prior attempts to do this have shown that, on the $Cu(643)^R$ surface, the kink density is 1.8 ± 0.1 nm^{-2}, slightly lower than the density of 2.03 nm^{-2} expected on the ideal surface.[22] Spectroscopic tools that could be more readily applied would be valuable, if of quantitative accuracy.

4.1. Thermal Distribution of Xe Adsorption Sites. It is clear from the Xe TPD spectra shown in Figure 5 that terrace, step, and kink adsorption sites cannot be titrated by Xe TPD. The only obvious impact of surface structure on the TPD spectra from the three Cu surfaces is the effect on the apparent order of the Xe desorption kinetics. The presence of steps on the high-Miller-index surfaces disrupts the formation of 2D islands of Xe and the resulting zeroth-order desorption kinetics observed on the Cu(111) surface. The differences between Xe adsorption energies on terrace, step, and kink adsorption sites are too small relative to the absolute Xe desorption energy to be readily observed by TPD. The low-coverage TPD spectra, shown in Figure 6, indicate that the differences in the Xe desorption energies from terrace, step, and kink sites are <5% of the desorption energy of $\Delta E_{des} = 22$ kJ/mol. The STM images of Figure 3 indicate that there is a significant degree of Xe detachment from the step edges at ~28 K. Thus, at the desorption temperature of ~80 K, Xe must be equilibrated predominantly on terrace sites, and one cannot observe resolvable TPD peaks for Xe desorption from the different sites. The distribution of Xe among sites at temperatures above 30 K is also revealed by the PAX spectra. The PAX spectra obtained from the Cu(221) surface at 50 K clearly show simultaneous population of the step and terrace sites as the coverage of Xe is increased from 0 to 1 ML. If the binding energy difference for Xe between step and terrace sites was sufficient, then at 50 K the Xe would sequentially populate the step sites at low coverage and then the terrace sites at higher coverages. At the temperatures at which the TPD and PAX data were obtained, all sites are populated simultaneously, with a thermal distribution of Xe among adsorption sites.

4.2. Xe Adsorption Site Distributions. Quantitative determination of the Xe adsorption site distributions requires fitting of the PAX spectra at each value of θ_{Xe} and on each Cu surface to determine the coverages of Xe adsorbed at terrace, step, and kink sites. The data set collected in this work is probably as comprehensive as those in any other reported study in terms of varying surface orientation and Xe coverage. In total, a set of

TABLE 1: PAX Fitting Parameters (eV)

site	$E_{5p1/2}$	w_i
terrace	7.28	0.174
step	7.39	0.343
kink	7.65	0.332

22 PAX spectra have been fit simultaneously using the same peak shapes and positions on all three surfaces and at all coverages. The spectra were background-subtracted using the spectra from the three clean Cu surfaces. The spectral fitting was applied to only the $5p_{1/2}$ peaks in the 7−8 eV binding energy range. Attempts to include the $5p_{3/2}$ peaks in the fitting process proved fruitless. Although the $5p_{3/2}$ spectra are clearly sensitive to the different site distributions on the three surfaces, their analysis is complicated by coverage-dependent peak shifts unrelated to adsorption site distributions.[48] The $5p_{1/2}$ peaks were fit on the three surfaces and at all coverages using a set of three Lorentzian peaks defined by three peak positions and three peak widths. The optimal values of these six parameters are listed in Table 1. The Xe $5p_{1/2}$ binding energy of 7.28 eV on the Cu(111) terraces is close to those of 7.1 and 7.2 eV reported elsewhere.[49,50] The widths of the Lorentzian functions used to fit the steps and kinks are clearly greater than that used for the terraces. This might reflect some inhomogeneity associated with the different types of step and kink sites that result from thermal roughening. The areas of the three peaks were then used to infer Xe population of different sites on the three Cu surfaces over the Xe coverage range of 0−1 ML. In this case, the monolayer is defined by the coverage at which the first signs of Xe adsorption in the second layer are observed or, in other words, saturation of the monolayer. On the Cu(111) surface, saturation of the monolayer occurs at a coverage corresponding at 1:3 ratio of Xe atoms to Cu atoms in the top layer of the Cu(111) surface.

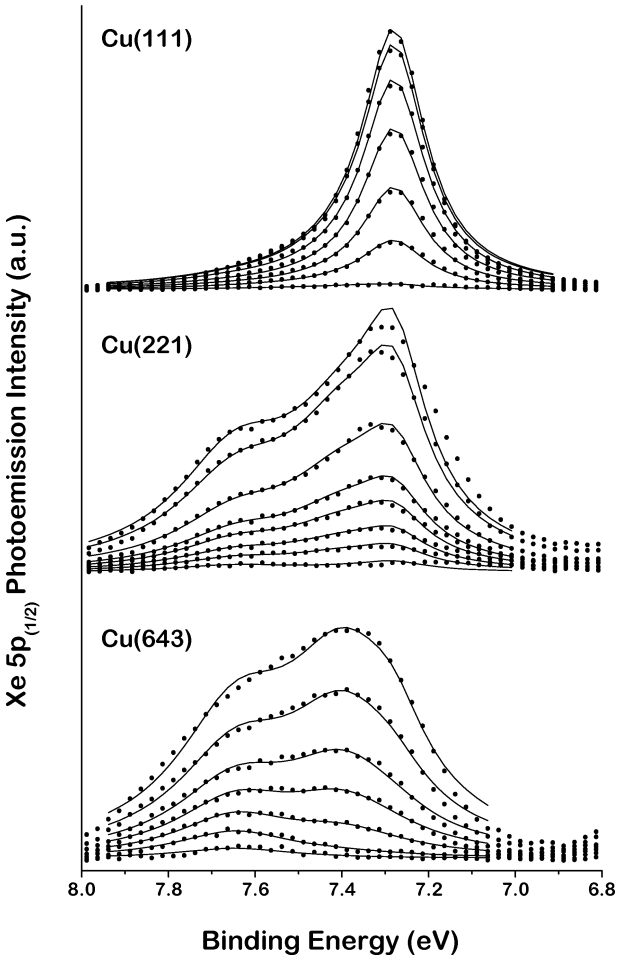

Figure 8. Fits of the PAX spectra on Cu(111), Cu(221), and Cu(643) using the six peak parameters in Table 1. The symbols are raw data points, and the solid lines are the spectral fits.

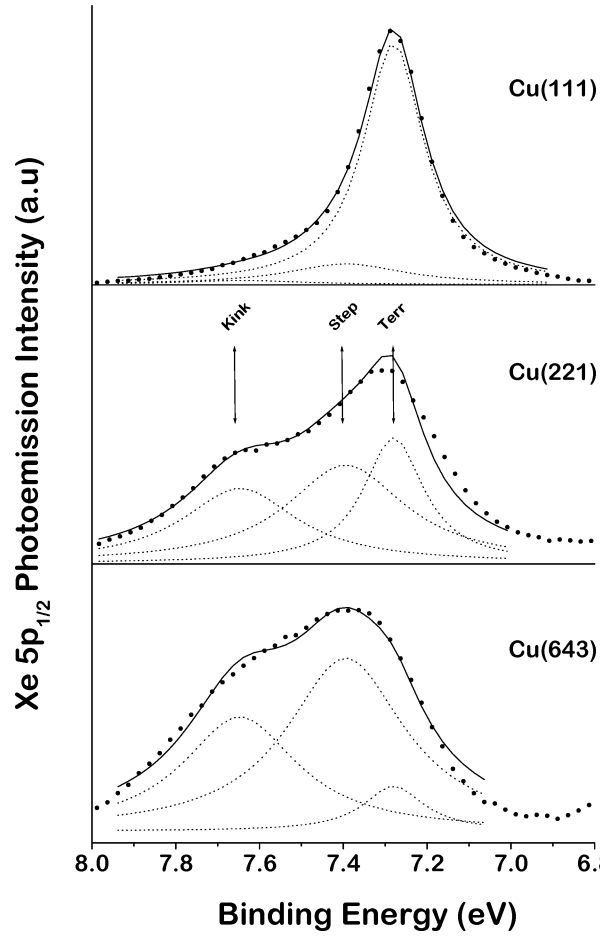

Figure 9. Fits of the PAX spectra at saturation Xe coverage on Cu(111), Cu(221), and Cu(643) using the six peak parameters in Table 1. The symbols are raw data points, and the solid lines are the spectral fits. The terrace, step, and kink components of each fit are shown in dashed lines.

Comparison of the raw data and the spectral fits reveals that the three Lorentzian peaks are adequate for fitting the Xe $5p_{1/2}$ spectra in the energy range of 7−8 eV. Figure 8 compares the fits for all coverages and on all three surfaces, showing the raw data as points and the fits as solid lines. Figure 9 illustrates the decomposition of the PAX spectra at the monolayer saturation coverage on all three surfaces into the three component peaks arising from Xe adsorbed on the terraces, steps, and kinks. Finally, Figure 10 illustrates the distribution of Xe among adsorption sites as functions of θ_{Xe} on all three Cu surfaces. The solid symbols denote fractional coverages determined using the six-parameter fit described above and illustrated in Figures 8 and 9. As expected, the Cu(111) surface is dominated by terrace sites. The fit suggests that ∼15% of the adsorbed Xe sits at step and kink sites. Given the relatively large size of Xe and the fact that it tends to pack in a $(\sqrt{3} \times \sqrt{3})R30°$ structure at saturation coverage on the Cu(111) surface,[46] this suggests that the step spacing on the Cu(111) surface is ∼12 unit-cell widths. This is a fairly high level of step defects and is certainly higher than that observed in the STM experiments or in our prior studies using (*R*)-3-methylcyclohexanone to titrate terrace,

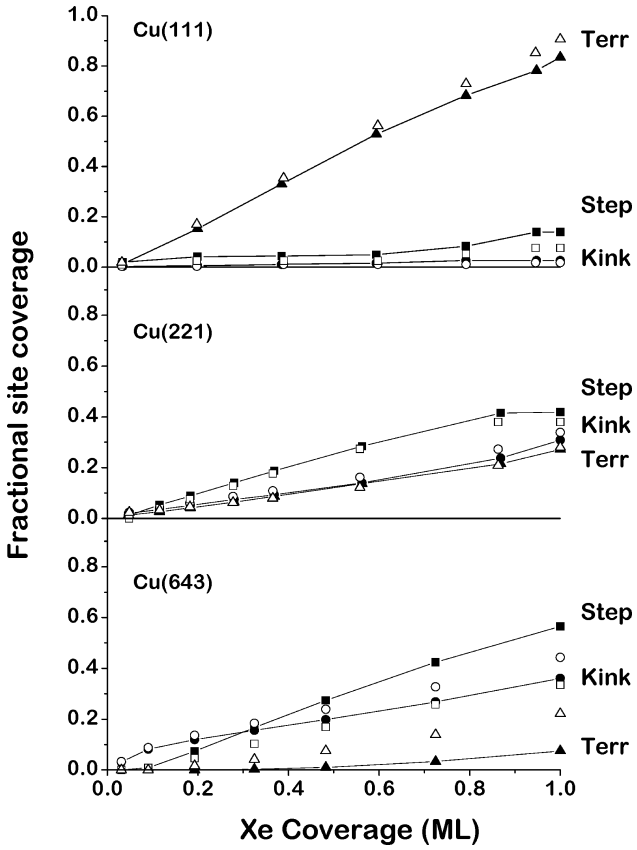

Figure 10. Xe coverages on terrace, step, and kink sites versus total θ_{Xe} determined from analysis of the PAX spectra obtained from the Cu(111), Cu(221), and Cu(643) surfaces at $T = \sim 55$ K. The solid symbols (■, step; ▲, kink; ●, terrace) are coverages obtained from the six-parameter fit using the parameter values listed in Table 1. The open symbols (□, step; Δ, kink; ○, terrace) were obtained from an 18-parameter fit in which the three peak energies and three peak widths were allowed to differ among the three surfaces.

step, and kink sites.[15] The open symbols in Figure 10 show the results of a spectral fit using 18 degrees of freedom that allows the terrace, step, and kink peak binding energies and peak widths to differ among the three surfaces but remain independent of coverage. This reduces the fraction of Xe at the steps and kinks to 9%, suggesting a step spacing of ~20 unit cells, still higher than observed using other probes. Examination of Figure 9 shows that the step and kink peaks generate intensity on the high-binding-energy side of the Xe $5p_{1/2}$ peak. The peak is slightly asymmetric. This intensity could arise from the presence of such sites on the Cu(111) surface but would also be very sensitive to the details of background subtraction. Thus, the general features of the analysis of the Xe $5p_{1/2}$ PAX spectra from the Cu(111) surface are reasonable, but the high-binding-energy asymmetry of the peak seems to overpredict the density of step and kink sites.

The ideal Cu(221) and the Cu(643) surfaces have steps that are spaced by ~2.5 times the close-packed row spacing of the Cu(111) terrace. On the Cu(111) terrace, Xe adsorbs in a $(\sqrt{3} \times \sqrt{3})R30°$ structure with a Xe row spacing that is 1.8 times the Cu row spacing. Given the need for spacing between the Xe and the step edge, this provides insufficient space for two close-packed rows of Xe atoms on the (111) terraces of the Cu(221) structure, except when the steps are nonideally spaced. The data for the Cu(221) surface in Figure 10 suggest that, at low coverage of Xe, the steps are filled at a slightly higher rate than the terrace sites. At saturation coverage, 27% of the Xe is adsorbed in terrace sites. This could be imagined if some fraction of the steps on the Cu(221) surface were wider than those of the ideal surface structure. What is surprising and seemingly unlikely in the fits of the PAX spectra from the Cu(221) surface is the density of kink sites, which rises to 31% at saturation of the Xe layer. Note that the results of the fitting process using 18 fitting parameters (open symbols) are not significantly different from those obtained with six fitting parameters (solid symbols). STM images of the Cu(533) surface, which has roughly the same step spacing as Cu(221), indicate that the steps are fairly straight.[51] The steps on Cu(533) are also close-packed but are (100) rather than (110) steps. The images taken at room temperature do indicate some thermal mobility of Cu atoms at room temperature, but the image of Cu(643) shown in Figure 1C and taken at 78 K shows that atomic motion has slowed significantly. It is questionable whether PAX is able to quantitatively resolve features from kinks versus straight step edges.

The step edges on the ideal Cu(643) surface have (110) kinks spaced by two unit-cell lengths of (100) step edge. The site distributions obtained from the PAX spectra reveal occupation of all three but suggest that the kink sites are occupied preferentially at low coverages. The terrace widths on Cu(643) are similar to those on Cu(221) and provide little room for adsorption of Xe on the (111) terraces. As measured at saturation Xe coverage using the six-parameter fit, the density of the step edge site is apparently slightly higher than that of the kink sites; however, the order switches when the 18-parameter fit is used. This again suggests that the PAX spectra cannot be used to quantitatively resolve the densities of step and kink sites.

5. Conclusions

STM, PAX, and TPD have been used to probe the adsorption site distributions of Xe on Cu(111), Cu(221), and Cu(643) surfaces. Whereas STM provides direct real-space images that can be used to quantify terrace, step, and kink site distributions, PAX and TPD methods are spectroscopic. The very small differences between the adsorption energies of Xe at the terrace, step, and kink sites on Cu preclude any use of the TPD spectra for quantification of site distributions. PAX provides a semi-quantitative tool for the determination of site distributions on the Cu surfaces. The PAX spectra are clearly sensitive to the surface structure and the presence of steps. However, PAX does not allow quantitative resolution of kink and step edge site densities.

Acknowledgment. All of the authors thank the NSF (CHE0717978 and CHE 1012307) for support of this research. H.L.T., A.E.B., and E.C.H.S. thank the donors of the American Chemical Society Petroleum Research Fund for additional support (Grant 45256-G5). A.E.B. thanks GAANN for the sponsorship of a one-year fellowship. We also thank Prof. K. Wandelt for a very helpful discussion.

References and Notes

(1) van Hove, M. A.; Somorjai, G. A. *Surf. Sci.* **1980**, *92*, 489–518.
(2) McFadden, C. F.; Cremer, P. S.; Gellman, A. J. *Langmuir* **1996**, *12*, 2483–2487.
(3) Sholl, D. S.; Asthagiri, A.; Power, T. D. *J. Phys. Chem. B* **2001**, *105*, 4771–4782.
(4) Ahmadi, A.; Attard, G.; Feliu, J.; Rodes, A. *Langmuir* **1999**, *15*, 2420–2424.
(5) Power, T. D.; Sholl, D. S. *Top. Catal.* **2002**, *18*, 201–208.
(6) Hazen, R. M.; Sholl, D. S. *Nat. Mater.* **2003**, *2*, 367–374.
(7) Sholl, D. S. *Langmuir* **1998**, *14*, 862–867.

(8) Bhatia, B.; Sholl, D. S. *Angew. Chem., Int. Ed.* **2005**, *44*, 7761–7764.
(9) Attard, G. A. *J. Phys. Chem. B* **2001**, *105*, 3158–3167.
(10) Hazzazi, O. A.; Attard, G. A.; Wells, P. B. *J. Mol. Catal. A: Chem.* **2004**, *216*, 247–255.
(11) Horvath, J. D.; Gellman, A. J. *J. Am. Chem. Soc.* **2001**, *123*, 7953–7954.
(12) Horvath, J. D.; Gellman, A. J.; Sholl, D. S.; Power, T. D. In *Enantiospecific Properties of Chiral Single Crystal Surfaces*; Hicks, J. M., Ed.; American Chemical Society: Washington, DC, 2000; pp 269−282.
(13) Horvath, J. D.; Gellman, A. J. *J. Am. Chem. Soc.* **2002**, *124*, 2384–2392.
(14) Horvath, J. D.; Gellman, A. J. *Top. Catal.* **2003**, *25*, 9–15.
(15) Horvath, J.; Kamakoti, P.; Koritnik, A.; Sholl, D. S.; Gellman, A. J. *J. Am. Chem. Soc.* **2004**, *126*, 14998–14994.
(16) Horvath, J. D.; Baker, L.; Gellman, A. J. *J. Phys. Chem. C* **2008**, *112*, 7637–7643.
(17) Greber, T.; Sljivancanin, Z.; Schillinger, R.; Wider, J.; Hammer, B. *Phys. Rev. Lett.* **2006**, *96*, 056103.
(18) Sljivancanin, Z.; Gothelf, K. V.; Hammer, B. *J. Am. Chem. Soc.* **2002**, *124*, 14789–14794.
(19) Rampulla, D. M.; Gellman, A. J. *Surf. Sci.* **2006**, *600*, 2823–2829.
(20) Rampulla, D. M.; Francis, A. J.; Knight, K. S.; Gellman, A. J. *J. Phys. Chem. B* **2006**, *110*, 10411–10420.
(21) Asthagiri, A.; Feibelman, P. J.; Sholl, D. S. *Top. Catal.* **2002**, *18*, 193–200.
(22) Baber, A. E.; Gellman, A. J.; Sholl, D. S.; Sykes, E. C. H. *J. Phys. Chem. C* **2008**, *112*, 11086–11089.
(23) Ertl, G.; Kuppers, J. *Low Energy Electrons and Surface Chemistry*, 2nd ed.; VCH Verlagsgesellschaft mbH: Weinheim, Germany, 1985.
(24) Puisto, S. R.; Held, G.; King, D. A. *Phys. Rev. Lett.* **2005**, *95*, 036102.
(25) Puisto, S. R.; Held, G.; Ranea, V.; Jenkins, S. J.; Mola, E. E.; King, A. A. *J. Phys. Chem. B* **2005**, *109*, 22456–22462.
(26) Jones, G.; Gladys, M. J.; Ottal, J.; Jenkins, S. J.; Held, G. *Phys Rev. B* **2009**, *79*, 165420.
(27) Giesen, M.; Dieluweit, S. *J. Mol. Catal. A: Chem.* **2004**, *216*, 263–272.
(28) Clegg, M. L.; Driver, S. M.; Blanco-Rey, M.; King, D. A. *J. Phys. Chem. C* **2010**, *114*, 4114–4117.
(29) Wandelt, K. *J. Vac. Sci. Technol. A* **1984**, *2*, 802–807.
(30) Wandelt, K.; Markert, K.; Dolle, P.; Jablonski, A.; Niemantsverdriet, J. W. *Surf. Interface Anal.* **1988**, *12*, 15–20.
(31) Jablonski, A.; Wandelt, K. *Surf. Interface Anal.* **1991**, *17*, 611–627.
(32) Wandelt, K. *Appl. Surf. Sci.* **1997**, *111*, 1–10.
(33) Bruch, L. W.; Diehl, R. D.; Venables, J. A. *Rev. Mod. Phys.* **2007**, *79*, 1381–1454.
(34) Da Silva, J. L. F.; Barreteau, C.; Schroeder, K.; Blugel, S. *Phys. Rev. B* **2006**, *73*, 125402.
(35) Da Silva, J. L. F.; Schroeder, K.; Bluegel, S. *Phys. Rev. B* **2004**, *70*, 245432.
(36) Da Silva, J. L. F.; Schroeder, K.; Blugel, S. *Phys. Rev. B* **2004**, *69*, 245411.
(37) Da Silva, J. L. F.; Schroeder, K.; Blugel, S. *Phys. Rev. B* **2005**, *72*, 033405.
(38) Da Silva, J. L. F.; Stampfl, C.; Scheffler, M. *Phys. Rev. B* **2005**, *72*, 075424.
(39) Park, J. Y.; Kahng, S. J.; Ham, U. D.; Kuk, Y.; Miyake, K.; Hata, K.; Shigekawa, H. *Phys. Rev. B* **1999**, *60*, 16934–16940.
(40) Schroder, U.; Linke, R.; Boo, J. H.; Wandelt, K. *Surf. Sci.* **1996**, *358*, 873–878.
(41) Weiss, P. S.; Eigler, D. M. *Phys. Rev. Lett.* **1992**, *69*, 2240–2243.
(42) Eigler, D. M.; Weiss, P. S.; Schweizer, E. K.; Lang, N. D. *Phys. Rev. Lett.* **1991**, *66*, 1189–1192.
(43) Eigler, D. M.; Schweizer, E. K. *Nature* **1990**, *344*, 524–526.
(44) Bouju, X.; Joachim, C.; Girard, C.; Sautet, P. *Phys. Rev. B* **1993**, *47*, 7454–7461.
(45) Stranick, S. J.; Kamna, M. M.; Weiss, P. S. *Science* **1994**, *266*, 99–102.
(46) Chesters, M. A.; Hussain, M.; Pritchard, J. *Surf. Sci.* **1973**, *35*, 161–171.
(47) Behm, R. J.; Brundle, C. R.; Wandelt, K. *J. Chem. Phys.* **1986**, *85*, 1061–73.
(48) Schmidt, K. J.; Christmann, K. *Surf. Sci.* **2003**, *525*, 159–172.
(49) Fusy, J.; Menaucourt, J.; Alnot, M.; Huguet, C.; Ehrhardt, J. J. *Appl. Surf. Sci.* **1996**, *93*, 211–220.
(50) Wandelt, K. Atomic Scale Surface Characterization by Means of PAX (Photoemission of Adsorbed Xenon). In *Chemistry and Physics of Solid Surfaces VIII*; Springer Series in Surface Sciences; Vanselow, R., Howe, R. F., Eds.; 1990; Vol. 22, pp 289−334.
(51) Zhao, X. Y.; Perry, S. S.; Horvath, J. D.; Gellman, A. J. *Surf. Sci.* **2004**, *563*, 217–224.

JP106489F